Clinical Neurophysiology 128 (2017) 1682–1695

Contents lists available at ScienceDirect

Clinical Neurophysiology

journal homepage: www.elsevier.com/locate/clinph

Synaptic damage underlies EEG abnormalities in postanoxic encephalopathy: A computational study

B.J. Ruijter [a,*], J. Hofmeijer [a,b], H.G.E. Meijer [c], M.J.A.M. van Putten [a,d]

[a] Clinical Neurophysiology, MIRA – Institute for Biomedical Technology and Technical Medicine, University of Twente, Hallenweg 15, 7522NB Enschede, The Netherlands
[b] Department of Neurology, Rijnstate Hospital, Wagnerlaan 55, 6815AD Arnhem, The Netherlands
[c] Applied Mathematics, MIRA – Institute for Biomedical Technology and Technical Medicine, University of Twente, Hallenweg 15, 7522NB Enschede, The Netherlands
[d] Departments of Neurology and Clinical Neurophysiology, Medisch Spectrum Twente, Koningsplein 1, 7512KZ Enschede, The Netherlands

ARTICLE INFO

Article history:
Accepted 15 June 2017
Available online 8 July 2017

Keywords:
Postanoxic encephalopathy
Electroencephalography
Synaptic failure
Short-term synaptic depression
Long-term potentiation
Mean field model

HIGHLIGHTS

- EEG evolution in postanoxic coma likely results from a gradual metabolic recovery of synapses.
- Specific postanoxic EEG patterns probably depend on long-term potentiation of excitatory synapses.
- Postanoxic generalized periodic discharges are refractory to treatment if potentiation of excitatory synapses is permanent.

ABSTRACT

Objective: In postanoxic coma, EEG patterns indicate the severity of encephalopathy and typically evolve in time. We aim to improve the understanding of pathophysiological mechanisms underlying these EEG abnormalities.
Methods: We used a mean field model comprising excitatory and inhibitory neurons, local synaptic connections, and input from thalamic afferents. Anoxic damage is modeled as aggravated short-term synaptic depression, with gradual recovery over many hours. Additionally, excitatory neurotransmission is potentiated, scaling with the severity of anoxic encephalopathy. Simulations were compared with continuous EEG recordings of 155 comatose patients after cardiac arrest.
Results: The simulations agree well with six common categories of EEG rhythms in postanoxic encephalopathy, including typical transitions in time. Plausible results were only obtained if excitatory synapses were more severely affected by short-term synaptic depression than inhibitory synapses.
Conclusions: In postanoxic encephalopathy, the evolution of EEG patterns presumably results from gradual improvement of complete synaptic failure, where excitatory synapses are more severely affected than inhibitory synapses. The range of EEG patterns depends on the excitation-inhibition imbalance, probably resulting from long-term potentiation of excitatory neurotransmission.
Significance: Our study is the first to relate microscopic synaptic dynamics in anoxic brain injury to both typical EEG observations and their evolution in time.

1. Introduction

Of all comatose survivors of cardiac arrest, 46–48% are alive and independent in activities of daily living after 6 months (Hofmeijer et al., 2015; Nielsen et al., 2013). Continuous electroencephalography (cEEG) in the first 24 h after resuscitation allows reliable identification of 50% of patients with either a good or poor outcome (Hofmeijer et al., 2015). Not only the EEG abnormalities as such, but also their timing and evolution are crucial indicators of the severity of the ischemic injury and prognosis (Tjepkema-Cloostermans et al., 2015). In the first days after an anoxic event, the EEG usually evolves in fixed sequences (Cloostermans et al., 2012; Jørgensen and Holm, 1998; Oh et al., 2015; Tjepkema-Cloostermans et al., 2015), and some EEG patterns are highly specific for postanoxic encephalopathy (Hofmeijer et al., 2013). Some of the transitions observed indicate good neurological recovery, whereas other have a strong association with a poor outcome.

* Corresponding author.
E-mail address: b.j.ruijter@utwente.nl (B.J. Ruijter).

http://dx.doi.org/10.1016/j.clinph.2017.06.245
1388-2457/

The common evolutional pathway for patients with a good outcome is from no measurable cortical activity (“isoelectric” EEG), via intermittent cortical activity (“burst-suppression EEG”) to continuous activity (Jørgensen and Holm, 1998). For patients with poor outcome, either a delayed evolution (Hofmeijer et al., 2015), or highly specific EEG patterns are observed. Examples of the latter are “burst-suppression with identical bursts” (Hofmeijer et al., 2013; Ruijter et al., 2015) and generalized periodic discharges (GPDs) on an isoelectric background (Ruijter et al., 2015). While these various EEG patterns and transitions can be related to patients' outcome, the pathophysiological mechanisms underlying these EEG abnormalities remain unclear.

EEG activity is mainly a reflection of cortical synaptic activity (Buzsáki et al., 2012). Therefore, EEG patterns observed in postanoxic encephalopathy reflect changes at the synaptic level, especially because synaptic failure is an early event observed in case of cerebral hypoxia (Hofmeijer et al., 2014; Hofmeijer and van Putten, 2012). A better understanding of synaptic mechanisms underlying the EEG in postanoxic encephalopathy will contribute to knowledge on the pathophysiology, and possibly open opportunities for treatment.

Neural mean field models can be used to relate microscopic properties of neurons to macroscopic network behaviour, reflected by EEG rhythms (Coombes, 2010; Deco et al., 2008). In such models, individual cell properties and their interactions are replaced by continuous functions that depend on some form of spatial averaging. Neural mean field models have been successfully used, for example, to simulate effects of anesthetics on the EEG (Bojak and Liley, 2005), epileptic seizures (Robinson et al., 2002), intermittent spike-wave dynamics (Goodfellow et al., 2011), and high-frequency oscillations (Wendling et al., 2002). With respect to postanoxic encephalopathy, a neural mean field model revealed a possible mechanisms underlying GPDs (Tjepkema-Cloostermans et al., 2014). However, other pathological EEG patterns, such as burst suppression with identical bursts (Hofmeijer et al., 2013), and pattern transitions as observed in postanoxic encephalopathy remain unexplained.

A relevant mechanism of synaptic failure in postanoxic encephalopathy is short-term synaptic depression, also called activity-dependent synaptic depression (Tsodyks and Markram, 1997): synapses need time to recover after signal transmission, for example to restore ion and neurotransmitter gradients. High neural firing rates limit the maximally achievable postsynaptic currents. This mechanism plays a role in physiological situations, and is probably aggravated in postanoxic encephalopathy. Specifically, this may be the result of presynaptic mechanisms, such as a dysfunction of plasma membrane Ca^{2+} extrusion systems comprised of Ca^{2+} pumps and Na^{+}/Ca^{2+} exchangers (Somjen, 2004) and a disturbed undocking of synaptic vesicles from the reserve pool attributable to impaired phosphorylation (Bolay et al., 2002). We assume that these effects are potentially reversible on a time scale of 24–72 h, in line with the typical recovery time of the EEG in postanoxic encephalopathy (Cloostermans et al., 2012; Jørgensen and Holm, 1998; Oh et al., 2015; Tjepkema-Cloostermans et al., 2015).

A second mechanism, taking place in severe postanoxic encephalopathy, is potentiation of excitatory neurotransmission. This mechanism has been substantiated by experimental observations in hippocampal slices exposed to anoxia (Miyazaki et al., 1993; Urban et al., 1989), and is compatible with the apparent network hyperexcitability in patients with severe postanoxic encephalopathy, reflected by a frequent observation of epileptiform discharges (Ruijter et al., 2015; Wijdicks and Young, 1994; Young et al., 1990). The most likely cause is anoxic long-term potentiation (LTP) of excitatory cortical synapses following anoxic depolarization (Calabresi et al., 2003; Hammond et al., 1994; Szatkowski and Attwell, 1994). This effect is caused by an increase of extracellular glutamate concentrations, resulting from reversed uptake of glutamate in neurons and glia cells (Rossi et al., 2000). In combination with anoxic depolarization, this induces a long-term potentiation of N-methyl-D-aspartate (NMDA)-receptor gated currents (Szatkowski and Attwell, 1994).

In this study, we aim to identify candidate synaptic mechanisms underlying typical EEG patterns and transitions in postanoxic encephalopathy by means of a neural mean field model. We hypothesize that, if synaptic recovery occurs in postanoxic encephalopathy, this is driven by a gradual improvement of short-term synaptic depression on a time scale of 24–72 h, and reflected by improvement of the EEG. Furthermore, we hypothesize that increasing severity of hypoxia leads to a stronger potentiation of excitatory synaptic transmission. We incorporated both these key mechanisms into our computational model. The simulated EEG patterns will be related to clinical EEG data of patients with postanoxic encephalopathy after cardiac arrest.

2. Methods

2.1. Clinical data collection

Continuous EEG recordings were collected between June 2010 and December 2015 in a large teaching hospital in The Netherlands (Medisch Spectrum Twente, Enschede). All patients who were admitted comatose after a cardiac arrest were included, if it was possible to start EEG recordings within 12 h after resuscitation. Two-thirds of the selected patients were also included in previous studies on outcome prediction after cardiac arrest (Cloostermans et al., 2012; Hofmeijer et al., 2015; Tjepkema-Cloostermans et al., 2015). Twenty-one silver/silver chloride cup electrodes were placed on the scalp according to the international 10–20 system. EEG recordings were continued until patients were awake or until the decision to withdraw treatment was made, with a maximum of five days. Additionally collected clinical data include age, gender, resuscitation details, and maximum levels of sedative medication. EEG data were not used for decisions regarding treatment withdrawal. However, treating physicians were not blinded to the EEG and treatment of electrographic seizures was left to the discretion of the treating physician. The primary outcome measure was the Cerebral Performance Category (CPC) at six months after cardiac arrest, assessed by a telephone interview. These scores were dichotomized into “good” (CPC 1–2, i.e. no or moderate neurological disability) and “poor” (CPC 3–5, i.e. severe disability, coma, or death). The Medical Ethics Committee Twente approved the protocol and waived the need for informed consent for EEG monitoring during the ICU stay and clinical follow-up.

2.2. Statistical analysis

In order to compare patients with good and poor outcomes, continuous variables were compared using independent samples t-tests and binary variables using X^2-tests. P-values < 0.05 were considered statistically significant.

2.3. Basic computational model

We used an adapted, spatially homogeneous version of the “bursting Liley model” (Bojak et al., 2015; Bojak and Liley, 2005; Liley et al., 2002) for our simulations. This model was used previously to simulate burst-suppression patterns (Bojak et al., 2015). Fig.1A gives an overview of the model. It consists of one population of excitatory (pyramidal) neurons and one population of inhibitory (inter-)neurons. Excitatory neurons have synaptic projections to

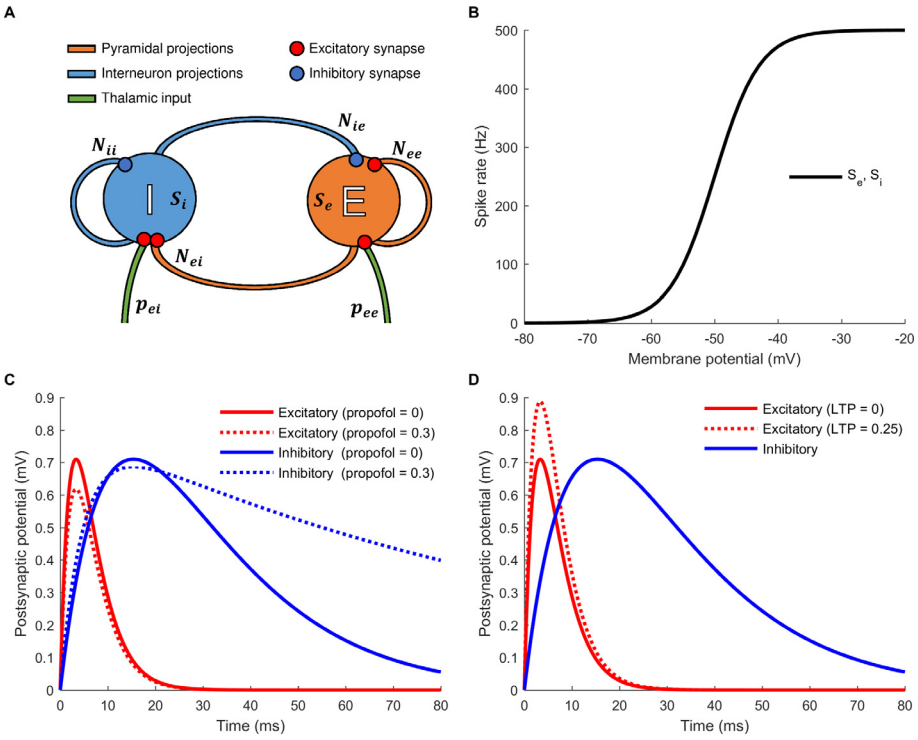

Fig. 1. Overview of computational model, including activation function and synaptic responses. A: Sketch of the spatially homogeneous Bursting Liley model. It comprises one excitatory population (E) and one inhibitory neural population (I). Excitatory synapses are indicated with red disks, inhibitory synapses with blue disks. The green lines indicate input from thalamic fibers. The symbols indicate the various inputs to the excitatory and inhibitor population, respectively. Details on these parameters can be found in Table A.1. B: The "activation function" for both the excitatory (E) and inhibitory (I) population, showing the relationship between mean membrane potential and population spiking rates. C: Synaptic response functions for excitatory (red) and inhibitory (blue) synapses. Curves represent the induced postsynaptic potential for a unit of presynaptic input. The continuous lines indicate the baseline response, the dashed lines the responses after application of a high dose of propofol. Note that we used a higher dose here (0.25 units) as compared to the simulations (0.15), in order to illustrate the effect. The peak values of the postsynaptic potential are referred to as Γ_e or Γ_i, respectively. D: Same synaptic response functions as in C, but with the dashed line indicating the excitatory response in case of long-term potentiation (LTP). (For interpretation of the references to colour in this figure legend, the reader is referred to the web version of this article.)

inhibitory neurons and to themselves. Similarly, inhibitory neurons have projections to excitatory neurons and to themselves. The spike rates of the neural populations depend on the mean membrane potential. In a hyperpolarized state, neurons will stop firing, and above a certain threshold potential firing rates will saturate to a maximum frequency (Fig.1B). All connections between neurons are synaptic connections. Postsynaptic membrane potentials are given by the convolution of the incoming firing rate with the "synaptic response function", as shown in Fig.1C and 1D. The peak amplitudes of the synaptic response functions are referred to as Γ_e and Γ_i for excitatory and inhibitory synapses, respectively.

The bursting Liley model includes short-term synaptic depression. This implies that the postsynaptic peak amplitudes Γ_e and Γ_i decrease as a function of presynaptic firing rates and recover with time constants τ_e^{rec} and τ_i^{rec}, respectively. Without noisy input from thalamic fibers, the average membrane potentials remain at some equilibrium value. For presynaptic firing rates above this equilibrium value postsynaptic peak amplitudes will decrease, and for presynaptic firing rates below the equilibrium value postsynaptic peak amplitudes will increase (see Appendix A for model details).

2.4. Adaptations to the bursting Liley model

To model the evolution of the EEG, we assumed the short-term synaptic recovery time constants τ_e^{rec} and τ_i^{rec} to vary slowly, on a time scale of hours. We hypothesize that, briefly after the anoxic event, these constants are very high ($\geq$100 times baseline value) and then slowly decay to their baseline values. This behaviour reflects the slow recovery of presynaptic metabolic processes in the postanoxic period. To model the effect of anoxic long-term potentiation of excitatory synapses, we increased the maximum amplitude of EPSPs (Γ_e). The effect is shown in Fig.1D. Candidate mechanisms include an increased expression of NMDA receptors or long-lasting elevations of modulators that potentiate NMDA-receptor opening, induced by the brief anoxic period (Szatkowski and Attwell, 1994). An alternative scenario, which we will not consider here, would be to increase the EPSP decay time, resulting in similar overall behaviour. In the following, we will indicate the fractional increase in Γ_e as the "LTP-factor", with a higher LTP factor indicating more severe hypoxic damage. Note that in the original bursting Liley model Γ_e is reduced and may recover with time constant τ_e^{rec} to its baseline value, while in our adaptation of the Liley model Γ_e may increase above its baseline value, reflecting excitatory potentiation. See Appendix A for details on the model equations.

2.5. Effects of anesthetic drugs

Most patients admitted to the Intensive Care Unit after a cardiac arrest are treated with targeted temperature management and sedation (Nielsen et al., 2013). In Medisch Spectrum Twente, patients are usually sedated with propofol. The bursting Liley model includes the effect of isoflurane, another general sedative agent. Fig.1C shows how sedation modifies the synaptic response function. Sedation increases the duration of inhibitory postsynaptic currents (IPSPs) and reduces the peak amplitude of excitatory postsynaptic currents (EPSPs). Although the model is quantita-

tively based on the effects of isoflurane, we assume propofol to have the same qualitative effects, since the $GABA_A$ receptor is the most important target site of both drugs (Garcia et al., 2010).

2.6. Numerical simulations

Differential equations were solved using the Euler-Maruyama method with a time step of 0.1 ms. For all simulations, we used the parameter values listed in Table A.1, unless stated otherwise. The basic set of parameters was chosen to generate a physiological alpha-rhythm (Liley et al., 2002; Tjepkema-Cloostermans et al., 2014).

In all simulations, EEG signals of 75 s were generated. The first 15 s of each simulation were ignored to exclude transient effects. The membrane potential $V_e(t)$ of the excitatory population was used to represent the EEG signal, as was done for example in (Bojak et al., 2015). The simulations thus resulted in a single time series, reflecting a single channel representation of the EEG. We considered this to be sufficient, since EEG abnormalities in postanoxic encephalopathy are typically spatially homogeneous.

Three parameters were varied in the simulations. Both the excitatory (τ_e^{rec}) and inhibitory (τ_i^{rec}) synaptic recovery time constants were varied between their baseline value (500 ms) and 10^7 ms. The chosen baseline value agrees with the physiological range of 250 ms to 1000 ms (Tsodyks and Markram, 1997). Because excitatory synapses probably recover slower than inhibitory synapses, we only considered simulations with $\tau_e^{rec} \geqslant \tau_i^{rec}$ as physiologically plausible (Khazipov et al., 1995; Tjepkema-Cloostermans et al., 2014). The LTP-factor was varied between 0 and 5. The order of magnitude for the LTP-factor was chosen based on experimental work in hippocampal slices after anoxia, where the maximum EPSP slope increased already twofold after 5 min of anoxia (Urban et al., 1989). Simulations were performed both without the effect of propofol and with a moderate dose of propofol (0.15 units), using Matlab (MATLAB and Statistics Toolbox Release R2015b, The MathWorks, Inc., Natick, Massachusetts, United States). The Matlab code used for the model simulations is included as Supplementary Material (Ruijter2017_model.m).

2.7. Categorization of clinical and simulated EEG data

EEG analysis was performed offline. Before any analysis, clinical EEG data were transformed to the longitudinal bipolar montage. Five minute artifact-free epochs were selected automatically every hour, as described previously in (Tjepkema-Cloostermans et al., 2013). Epochs were filtered using a sixth order zero-phase Butterworth bandpass filter with cutoff frequencies of 0.5 and 25 Hz. Categorization was solely based on quantitative analysis. Epochs were categorized into one of six categories: normal, low-voltage, discontinuous, burst-suppression, irregular discharges, and periodic discharges. Categorization was based on four features: continuity, burst-suppression contrast ratio, frequency of epileptiform discharges, and regularity epileptiform of discharges. Continuity was defined as the fraction of signals free of "suppressions" (Ruijter et al., 2015). Suppressions were defined as segments with duration of at least 0.5 s with all amplitudes below 10 μV. The burst-suppression contrast ratio was calculated if continuity was 10–90% and was defined as the power ratio between "bursts" and "suppressions". Quantitative values were derived per channel, after which the median value was calculated. Discharges were detected using the algorithm described in (Ruijter et al., 2015). Only generalized discharges, occurring in more than 9 channels simultaneously, were taken into account. If the detected discharge frequency exceeded 0.5 Hz, an irregularity index was calculated, defined as the standard deviation of the inter-discharge intervals divided by the mean inter-discharge interval. Epochs were classified as normal if continuity was higher than 90% and the discharge frequency was below 0.5 Hz. Epochs with continuity below 10% were classified as low-voltage. Epochs with 10–90% continuity were classified as burst-suppression if the burst-suppression contrast ratio was 3.5 or higher, and as discontinuous if the burst-suppression contrast ratio was lower than 3.5. In case of epileptiform discharges with frequency of 0.5 Hz or higher, epochs were either classified as irregular discharges or as periodic discharges, depending on the irregularity parameter. Fig. 2, in the results section, shows detailed criteria, including representative examples of clinical data and simulated EEG for each of the categories.

In order to facilitate a direct comparison with clinical EEG data, simulated EEG was filtered and categorized using the same algorithm. Simulated signals were treated as if they were single channel representations of EEG. Therefore, all detected suppressions and discharges in the simulated data were treated as if they were generalized.

3. Results

3.1. Patients

A total of 155 patients were included. Seventy-one had a good neurological outcome (CPC 1–2), 84 had a poor neurological outcome (CPC 3–5) after 6 months. Table 1 shows baseline characteristics of the included patients. As expected, patients with a good neurological outcome were younger (61 vs. 66 years, $p = 0.025$), less often had a noncardiac cause of the arrest (6% vs. 26%, $p < 0.001$), and more often ventricular fibrillation (VF) as initial cardiac rhythm (93% vs. 60%, $p < 0.001$). Patients with good outcomes had higher sedative requirements with propofol (3.24 vs 2.71 mg/kg/h, $p = 0.004$), fentanyl (1.94 vs. 1.53 μg/kg/h, $p = 0.002$), and remifentanil (7.35 vs. 4.29 μg/kg/h, $p = 0.033$). Bilaterally absent N20 responses on a median nerve SSEP were found in 38% of patients with a poor outcome, and in none of the patients with a good outcome. There was no statistically significant difference between patients with good and poor outcomes with respect to gender, location of cardiac arrest, treatment with hypothermia, and EEG start or end times.

3.2. Evolution of clinical EEG data

Fig. 3 schematically summarizes the EEG evolution of all patients. A few representative cases are shown in Fig. 4. We have grouped patients according to similarities in their evolutional patterns. In 117 cases (75%) the initial EEG was low-voltage. The largest subset (Fig. 3A) includes 87 patients. These cases fit into a sequence from low-voltage, via discontinuous to normal EEG. Note that 63 (72%) of these cases had a good outcome, and that the chance of a good outcome was higher if there was an early transition from low-voltage to a discontinuous and normal EEG. Cases in Fig. 3B and C evolve from low-voltage to discontinuous EEG and, at some point to epileptiform discharges. Fig. 3B includes patients with only irregular discharges, Fig. 3C also includes patients with periodic discharges. Eight cases (40%) in Fig. 3B had a good outcome, while none of the patients in Fig. 3C survived. For cases in Fig. 3D and E the common transition is from low-voltage to burst-suppression EEG. Cases in Fig. 3D do, at some point in time, improve beyond burst-suppression, and cases in Fig. 3E do not evolve to other patterns. None of the cases in Fig. 3D and E survived. Fig. 3F includes cases that showed only a low-voltage EEG. None of these 11 patients had a good outcome. Note that, for all groups together, 33 of 34 patients with a 'normal' EEG within 30 h after cardiac arrest had a good outcome. Case 143, who died

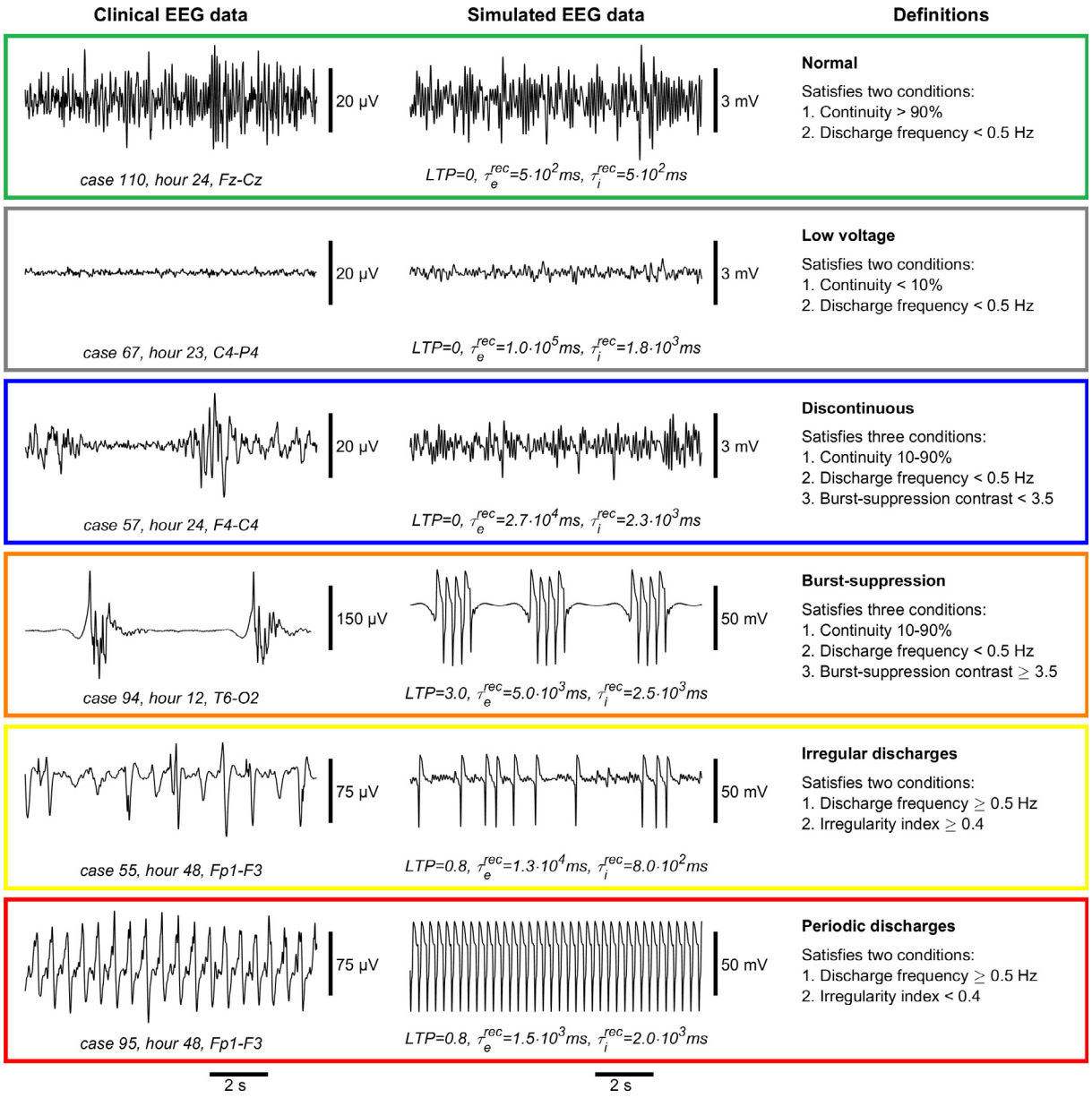

Fig. 2. Overview of category definitions, including representative examples of clinical and simulated EEG data. The first column shows 10-s, one channel representations of clinical EEG data. Below each sample, the case number, hours since cardiac arrest, and bipolar derivation are shown. For each example, the best possible bipolar derivation was chosen based on visual inspection. The second column shows representative simulated EEG patterns. The parameters used are shown below each simulation. The third column provides category definitions. Colors shown correspond to the colors used in Figs. 3–6. Note that we allowed for discharges of frequency < 0.5 Hz to occur in normal, low-voltage, or discontinuous patterns. (For interpretation of the references to colour in this figure legend, the reader is referred to the web version of this article.)

as a result of respiratory problems, is the only exception. Further note that all 14 patients with no other EEG pattern than low-voltage in the first 35 h had a poor outcome.

3.3. Simulations

Within the allowed range of parameters, the model generates all of the six categories of EEG patterns listed in Fig. 2. The category of EEG pattern depends strongly on the synaptic recovery time constants, LTP-factor, and propofol dose. Fig.5A shows the spectrum of possible EEG patterns for various LTP-factors, with and without administration of propofol. The parameter planes are composed of the recovery time constants for excitatory synapses (τ_e^{rec}) and inhibitory synapses (τ_i^{rec}), for a fixed value of the LTP-factor. When time progresses and energy supply is restored, τ_e^{rec} and τ_i^{rec} will eventually recover towards their baseline values in the lower left corner. Because we assume that excitatory synapses are metabolically more severely affected than inhibitory synapses, only the non-shaded areas ($\tau_e^{rec} > \tau_i^{rec}$) are considered physiologically plausible. Besides, parameter values in the shaded areas ($\tau_e^{rec} < \tau_i^{rec}$) did not lead to plausible patterns and transitions.

The introduction of LTP changes the range of possible EEG patterns. With LTP = 0, the EEG will be normal when the synaptic recovery time constants τ_e^{rec} and τ_i^{rec} are close to their baseline values. For larger values of the synaptic recovery time constants, discontinuous or low-voltage patterns are possible, as well. For increasing LTP-factor, subsequently, irregular discharges, periodic discharges, burst-suppression, and low-voltage EEG move into the spectrum of possible EEG patterns. This indicates that for higher LTP-values it becomes more likely for the EEG to be in

Table 1
Baseline characteristics of the patients included.

Characteristic	Good outcome (CPC 1–2)	Poor outcome (CPC 3–5)	P-value
Number of patients	71 (46%)	84 (54%)	
Age	61 (29–88)	66 (21–86)	0.025
Female	21 (30%)	26 (31%)	0.850
OHCA	64 (90%)	67(80%)	0.080
Noncardiac cause	4 (6%)	19 (26%)	<0.001
VF as initial cardiac rhythm	63 (93%)	46 (60%)	<0.001
Treated with hypothermia (33 C)	71 (100%)	83 (99%)	0.360
Patients treated with propofol	70 (99%)	82 (98%)	0.669
Max. propofol rate (mg/kg/h)	3.24 (0.24–7.54)	2.71 (0.89–7.00)	0.004
Patients treated with midazolam	17 (24%)	18 (21%)	0.710
Max. midazolam rate (μg/kg/h)	65 (27–125)	69 (29–143)	0.739
Patients treated with fentanyl	57 (80%)	63 (75%)	0.430
Max. fentanyl rate (μg/kg/h)	1.94 (0.67–3.33)	1.53 (0.63–4.71)	0.002
Patients treated with remifentanil	13 (18%)	18 (21%)	0.630
Max. remifentanil rate (μg/kg/h)	7.35 (2.50–14.7)	4.29 (1.11–13.3)	0.033
Median nerve SSEP	26 (37%)	63 (75%)	<0.001
Bilaterally absent N20 response	0 (0%)	24 (38%)	<0.001
EEG start time (hours)	6 (2–11)	6 (3–11)	0.795
EEG end time (hours)	68 (27–142)	66 (5–223)	0.661

Numbers are displayed as mean (range), unless otherwise indicated. P-values were calculated with independent samples t-test for continuous variables and with X^2-test for binary variables. EEG start and end times are relative to the time of resuscitation. OHCA: out of hospital cardiac arrest.

one of these pathological states. If propofol is added, effects of the increased LTP-factor are partially or completely reversed. This means, for example, that in case of periodic discharges, adding propofol results in a normal or discontinuous EEG. However, if the LTP-factor does not change during treatment, these pathological patterns will reappear after propofol treatment has ended.

Fig.5B shows representative examples of the simulated EEG patterns. Note the difference between patterns 2a and 2b, both classified as low-voltage. In example 2a, from the lower right area of the parameter space, there is still some visible activity. A closer inspection of the unfiltered signals indicates that this pattern results from hyperpolarization, i.e. the mean excitatory membrane potential $V_e(t)$ is below its equilibrium value. In example 2b, generated in the upper left area of the parameter space, EEG activity is almost completely suppressed. Here, low-voltage EEG results from depolarization, i.e. the mean excitatory membrane potential $V_e(t)$ is (far) above its equilibrium value. Further note that "discontinuous" patterns in the simulations have no suppressions, like the clinical example in Fig. 2, but are rather an amplitude intermediate between low-voltage and normal EEG patterns.

3.4. Temporal evolution of simulated EEG patterns

In the following, we will relate the possible evolution of simulated EEG to the evolutional pathways of clinical data as shown in Fig. 3. We assume that briefly after the anoxic event, short-term synaptic recovery time constants τ_e^{rec} and τ_i^{rec} are significantly increased. When synapses recover from the anoxic injury, these time constants will slowly return to their baseline values, indicated by the black circles in Fig.5A. The EEG will therefore always evolve in this direction, if we ignore effects of permanent failure of synapses or neural cell death.

Fig. 6 shows four possible evolutional trajectories of the EEG, corresponding to the subsets of clinical EEG data in Fig. 3. The observations in clinical EEG data suggest that in most cases the initial EEG pattern is low-voltage. Therefore, all chosen pathways start in a low-voltage area. Pathway A leads to the sequence low-voltage – discontinuous – normal. This pathway is most likely to occur without LTP (LTP = 0). Pathway B is similar to pathway A, and eventually the EEG displays irregular discharges. This pathway requires a slightly higher LTP value (LTP = 0.25). For a moderate LTP-value (0.8), evolution to periodic discharges is possible (Pathway C). Pathways D and E both include the transition from low-voltage to burst-suppression EEG. This transition is only possible for high LTP-values (LTP $\geq$ 2). Note that burst-suppression can only occur in case of high values of the synaptic recovery time constants τ_e^{rec} and τ_i^{rec}. This indicates that both aggravated short-term synaptic depression and potentiation of excitatory neurotransmission are required for burst-suppression patterns. See Appendix B for a mathematical description (in terms of bifurcations) of the transitions between the simulated EEG patterns.

3.5. Comparison between clinical data and simulations

If we assume that both the LTP-factor in simulations and CPC-scores in patients are measures for the severity of hypoxic injury, there are striking similarities between the simulations and the clinical EEG data. Patients had the highest (75%) chance for a good neurological outcome if their EEG evolved in the sequence low-voltage – discontinuous – normal (Fig.3A). In the model simulations, this type of evolution was only possible for low or absent LTP. Patients who evolved to irregular discharges from a discontinuous or normal EEG (Fig.3B) had a moderate chance of a good outcome (40%). In the model simulations, this evolutional pathway was most likely to occur for intermediate LTP values. None of the patients with periodic discharges (Fig.3C), or patients who evolved from low-voltage to burst-suppression patterns (Fig. 3D and E) had a good outcome. In the simulations, these patterns were only possible for high or very high LTP-factors.

Fig. 3 suggests that not only the sequence of EEG patterns determines the outcome, but also the speed by which the EEG evolves through the transitions. From Fig.3A, for example, follows that patients more likely had a poor outcome if they spent more time in low-voltage EEG. In terms of the model, there are two possible explanations. The first possibility is that the initial synaptic time constants in these patients are far away from their baseline values ($\tau_e^{rec} \gg \tau_{e,0}^{rec}$ or $\tau_i^{rec} \gg \tau_{i,0}^{rec}$), indicating that the synaptic metabolism initially is severely affected. The second possibility is that the rate of synaptic recovery in these patients (i.e. the speed of decay of τ_k^{rec} towards $\tau_{k,0}^{rec}$) is slower.

Finally, it was not possible to categorize patients from Fig.3F into one of the evolutional pathways of the model. Their low-voltage patterns can either be the result of hyperpolarization, (indicating mild hypoxic injury), depolarization (indicating severe

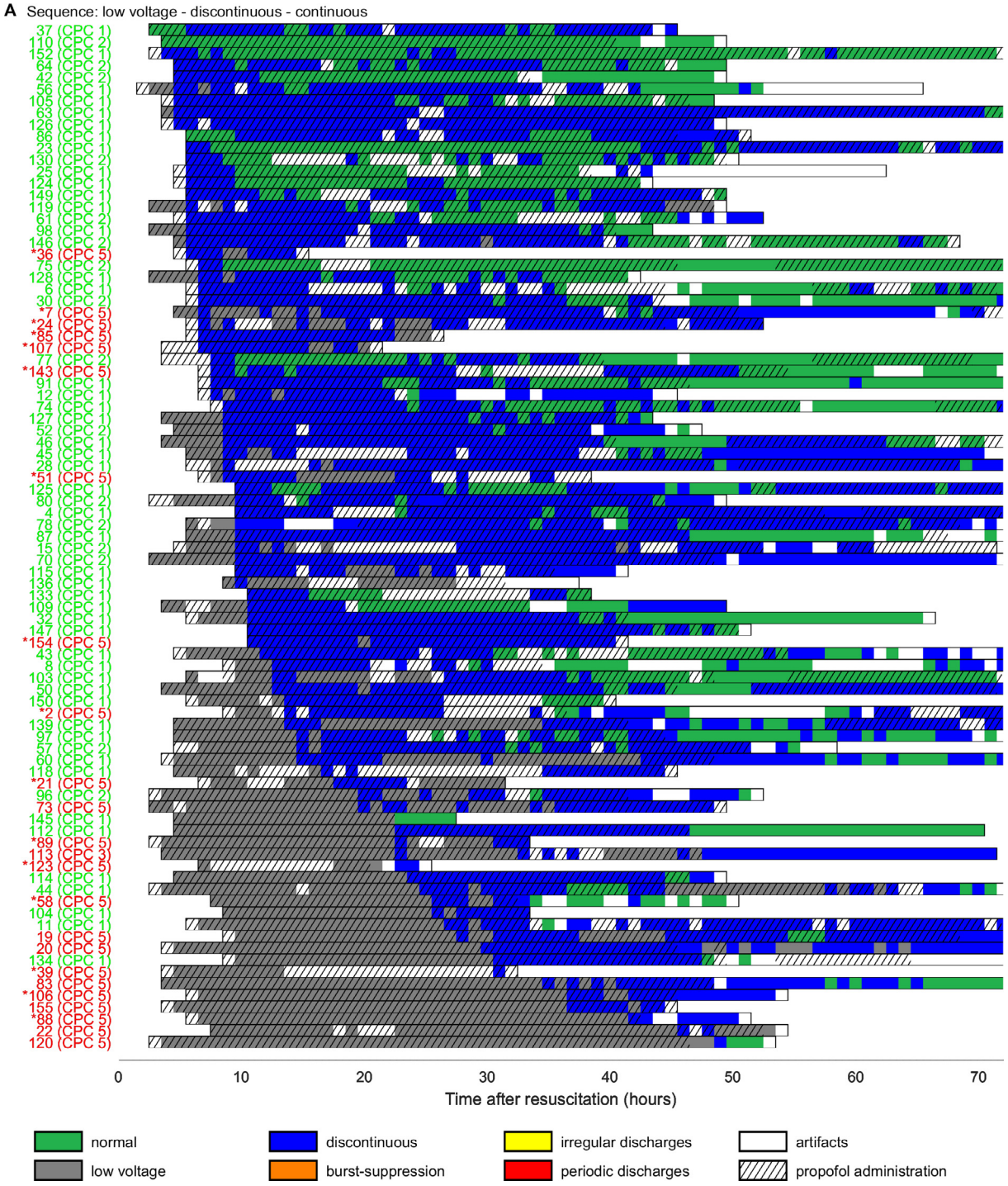

Fig. 3 (part 1). Evolution of clinical EEG data. Each row represents one case, and is preceded by the case number and CPC-score after 6 months. Cases with good outcomes are shown in green, cases with poor outcomes in red. Data points are shown per hour, and are based on quantitative analysis of a 5-min artifact-free epoch. Only data of the first 72 h after cardiac arrest are shown here. Hatched areas indicate that EEG was recorded during propofol administration. Cases have been grouped by common characteristics in the evolution of their EEG. Within groups, cases have been sorted by the timing of the first non-low-voltage EEG pattern. Cases numbers preceded by '*' died as a result of a second cardiac arrest, respiratory problems, or hemodynamic instability. In all other cases who died (CPC = 5), life-supporting treatment was withdrawn, at least partially based on the (suspected) poor neurological prognosis. A: cases with EEG sequence from low-voltage, via discontinuous to normal. (part 2). B: cases evolving from low-voltage, via discontinuous EEG to irregular discharges. C: cases evolving from low-voltage, via discontinuous EEG to periodic discharges. D: cases evolving from low-voltage, via burst-suppression, to other patterns. E: cases with sequence low-voltage - burst-suppression – low-voltage. F: cases in whom no other pattern than low-voltage EEG was detected. Note that midazolam was used as sedative medication instead of propofol in case 26 from hour 6 to 72, and in case 101 from hour 5 to 22. (For interpretation of the references to colour in this figure legend, the reader is referred to the web version of this article.)

anoxic injury), or irreversible synaptic failure (also indicating severe anoxic injury). Regarding the fact that all these patients had a poor neurological outcome, depolarization and irreversible synaptic failure are most likely.

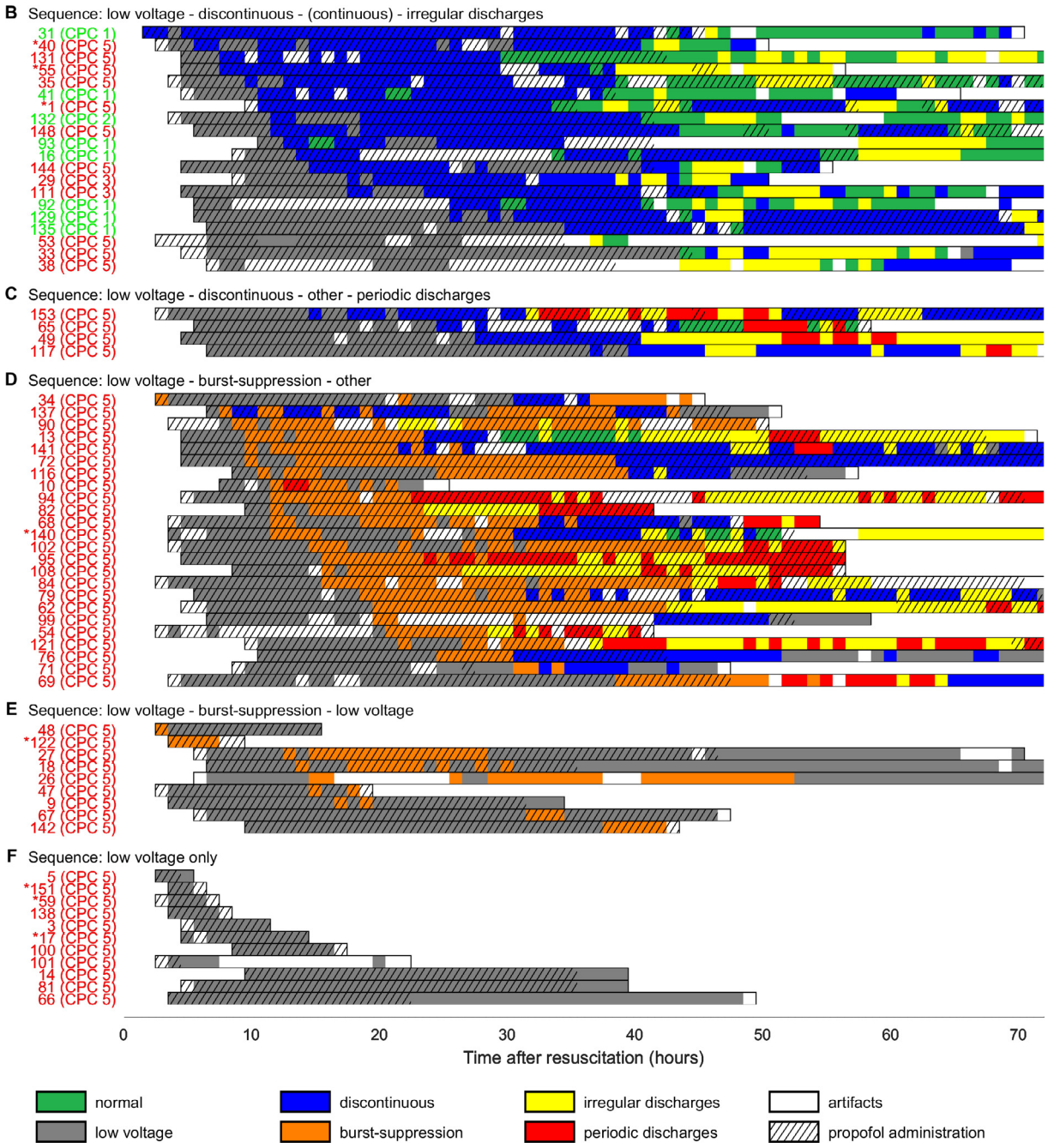

Fig. 3 (part 2). (*continued*)

4. Discussion

In this study, we used a mean field computational model to explain pathological EEG patterns for various grades of severity of postanoxic encephalopathy. The model incorporates mechanisms that modify the dynamics of synapses. It successfully reproduces commonly observed EEG patterns such as the physiological alpha rhythm, burst-suppression patterns, irregular and periodic discharges, and low-voltage EEG. In addition, the model correctly predicts some of the common evolutionary pathways of the EEG. In situations with mild hypoxic injury, reflected by a low LTP-factor, it correctly predicts the transition from low-voltage EEG, via discontinuous patterns, to normal EEG patterns. For severe injury, reflected by a high LTP-factor, it predicts the transition from low-voltage patterns to burst-suppression patterns and periodic discharges, without improvement to normal EEG patterns. This indicates that anoxic long-term potentiation of excitatory neurotransmission and a transient aggravation of short-term synaptic depression are plausible pathophysiological mechanisms of postanoxic encephalopathy. Furthermore, our findings support the notion that excitatory synapses are more severely affected by anoxic injury than inhibitory synapses.

Although some of the observed patterns, such as periodic discharges and burst-suppression, have been simulated successfully before (Bojak et al., 2015; Tjepkema-Cloostermans et al., 2014), the dynamics of EEG evolution in postanoxic encephalopathy,

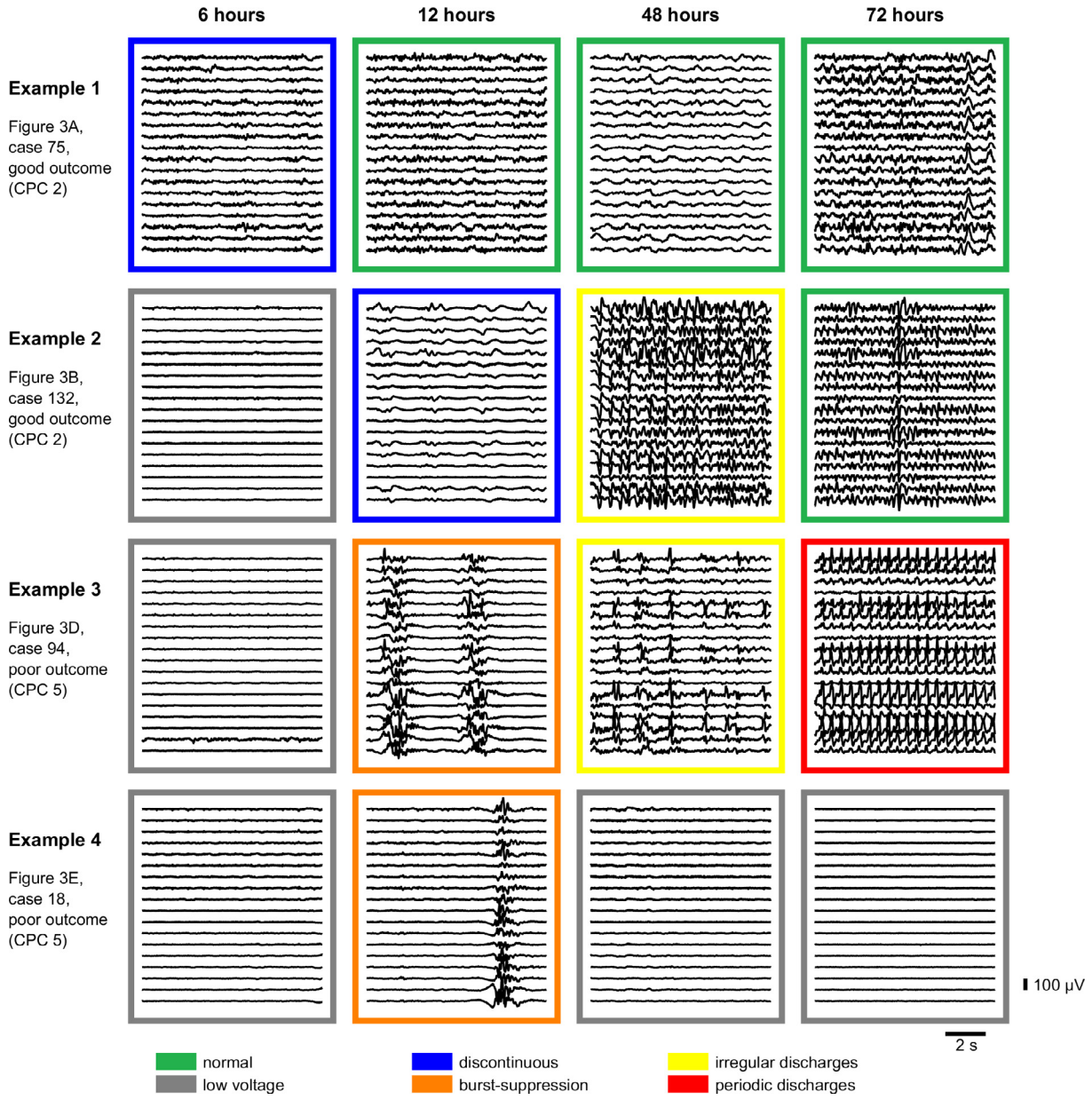

Fig. 4. Representative examples of the evolution of clinical EEG-data. The first example (case 75, Fig. 3A) readily improves from a discontinuous to a continuous, diffusely slowed pattern and thereafter remains continuous throughout the recording. The second example (case 132, Fig. 3B), evolves from low-voltage to a continuous pattern and then shows a transient period with irregular discharges, a few hours after treatment with propofol was stopped. The third example (case 94, Fig. 3D) is initially isoelectric and evolves via burst-suppression with identical bursts to generalized period discharges. The last example (case 18, Fig. 3E) evolves from isoelectric to burst-suppression and eventually to a low-voltage EEG.

including typical transitions between various EEG patterns, were never addressed.

4.1. Role of short-term synaptic depression

Previous research indicates that aggravated short-term synaptic depression is most likely the result of presynaptic mechanisms, such as a dysfunction of plasma membrane Ca^{2+} extrusion systems (Somjen, 2004) and a disturbed undocking of synaptic vesicles attributable to impaired phosphorylation (Bolay et al., 2002). Although a depletion of ATP could account for these effects, this is not likely. Simultaneous measurements of EEG and ATP levels in rat brains indicate that ATP level recovery is much faster than functional recovery as measured with EEG (Ljunggren et al., 1974; Naruse et al., 1984). However, some of the amino acid levels associated with the citric acid cycle may remain abnormal for a prolonged period (Ljunggren et al., 1974) and secondary mitochondrial failure may occur (Siesjö et al., 1999). Another potential mechanism is the failure of neural protein synthesis. In animal experiments, it has been shown that protein synthesis recovers on a time scale of 24 h after the anoxic event (Bodsch et al., 1986), which is essentially the same time scale on which the EEG recovers.

Because the net effect of short-term synaptic depression is a decrease of postsynaptic currents (PSPs), other mechanisms that decrease PSPs, such as a decrease in the number of postsynaptic neurotransmitter receptors, may also lead to some of the effects observed. Low-voltage patterns, for example, can be explained by such a mechanism. However, short-term synaptic depression has the advantage that it also facilitates periodic patterns, by means

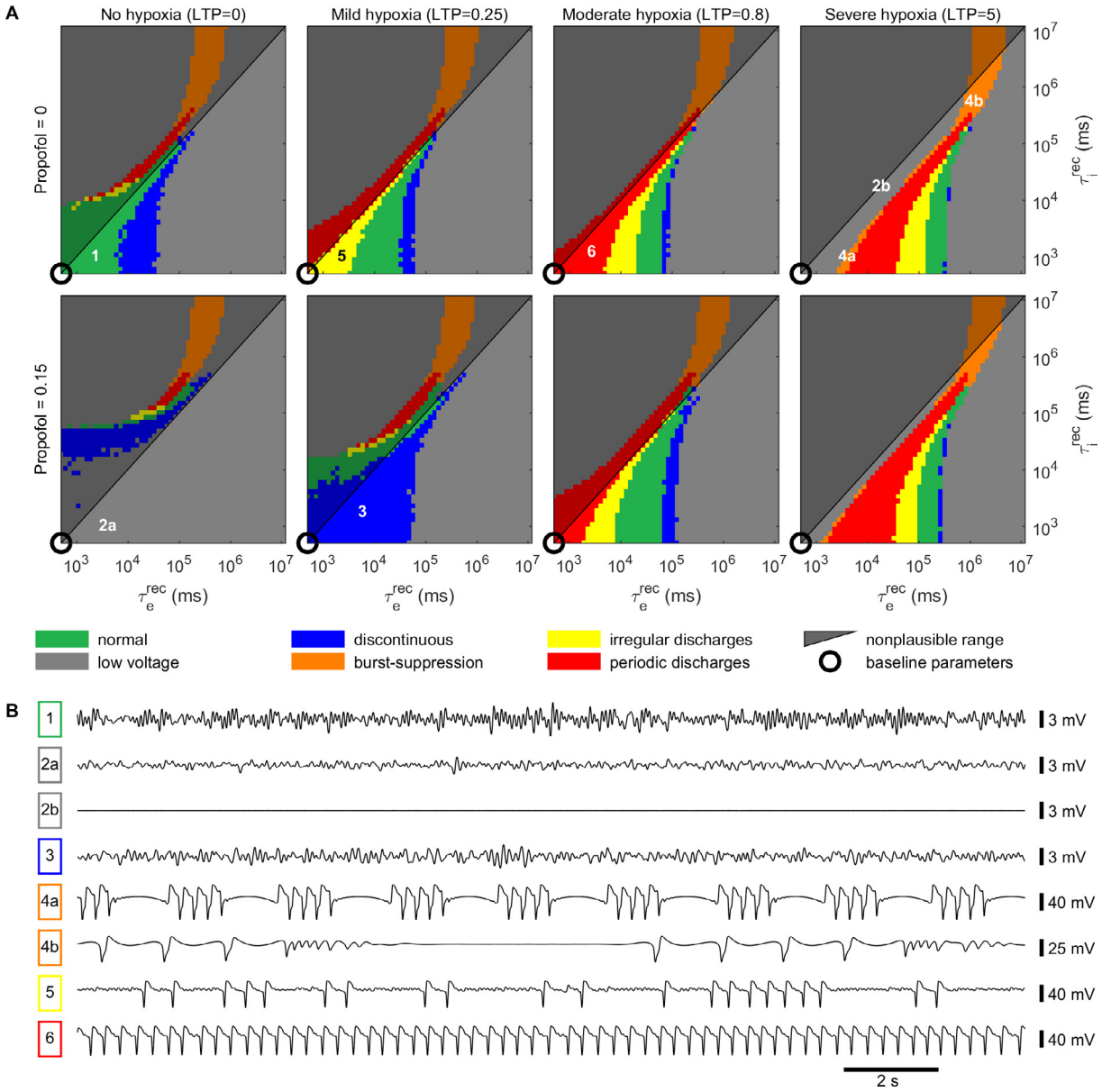

Fig. 5. Overview of the simulations for different scenarios, with LTP ranging from LTP = 0 to LTP = 5, and with and without propofol. A: Overview of possible EEG patterns in various regions of the parameter space. The consecutive columns represent an increasing grade of anoxic injury, reflected by increasing LTP-values from left to right. The upper row represents the situation without propofol, the lower row the situation with a moderate dose (0.15 units) of propofol. Only the non-shaded area, where excitatory neurotransmission is more severely affected than inhibitory neurotransmission, is considered physiologically plausible. The numbers in the subplots refer to the examples in panel B. The black circle in the bottom left corner is put around the baseline value of the synaptic recovery time constants. B: Representative examples of simulated EEG patterns.

of its feedback-loop (Bojak et al., 2015; Liley and Walsh, 2013; Tabak et al., 2000). Our findings indicate that excitatory synapses are more strongly affected by effects of activity-dependent synaptic depression than inhibitory synapses. Simulations with equal recovery times for excitatory and inhibitory synapses, or with longer recovery times for inhibitory synapses, did not produce any plausible results.

The model observation that increasing severity of ischemic damage results in a slower restoration of background continuity is in line with previous findings. In studies on the prognostic value of continuous EEG in postanoxic encephalopathy it was found that continuous EEG activity within 12 h after cardiac arrest indicates a good outcome, whereas outcome is always poor is there if still no measurable EEG activity after 24 h (Hofmeijer et al., 2015). Note that these findings on timing of EEG patterns in relation to outcome differ slightly from our results, as we used a stricter, quantitative definition for continuity of the EEG.

4.2. Potentiation of excitatory neurotransmission

Our results indicate that anoxic long-term potentiation of excitatory synapses is a plausible mechanism underlying certain pathological EEG patterns observed in postanoxic encephalopathy. It is compatible with the apparent network hyperexcitability in patients with severe postanoxic encephalopathy, reflected by a frequent observation of epileptiform discharges (Wijdicks and Young, 1994; Young et al., 1990). Since anoxic long-term potentiation is independent of Ca^{2+} dependent presynaptic neurotransmitter release, there is no paradox between synaptic depression and a rise in extracellular glutamate levels (Ikeda et al., 1989; Martin et al.,

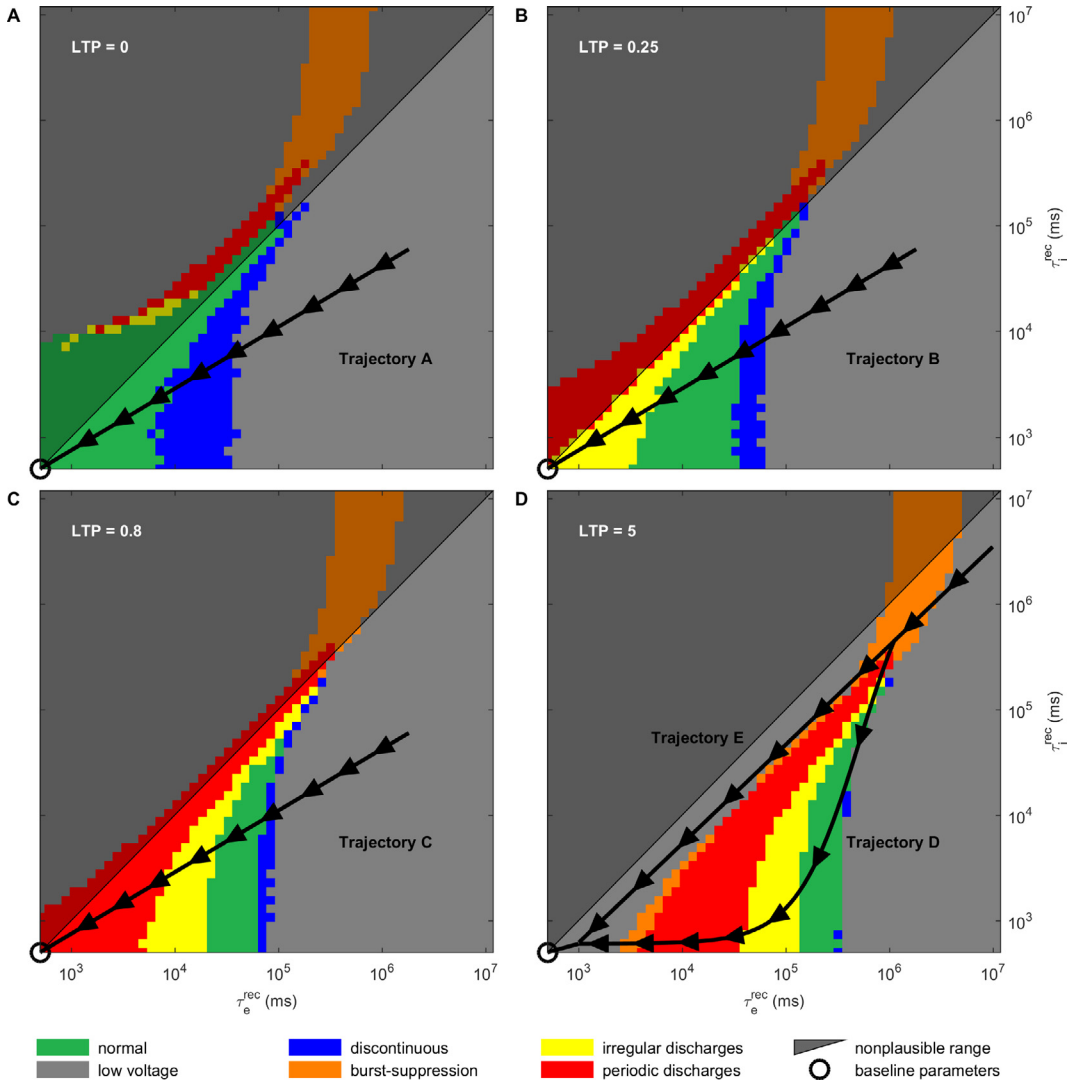

Fig. 6. Possible evolutional pathways of the simulated EEG, shown as through the parameter plane. The letters used correspond to the evolutional pathways of clinical data in Fig. 3. A: Parameter plane in case of no LTP (LTP = 0). Trajectory A leads to a sequence from low-voltage, via discontinuous to normal EEG, like the clinical cases in Fig. 3A. B: Parameter plane for mild hypoxic injury (LTP = 0.25). Trajectory B leads to the sequence low-voltage – discontinuous – normal – irregular discharges, corresponding to Fig. 3B. C: Parameter plane for moderate hypoxic injury (LTP = 0.8). Trajectory C leads to the sequence low-voltage – discontinuous – normal – irregular discharges – periodic discharges, corresponding to Fig. 3C. D: Parameter plane for severe hypoxic injury (LTP = 5). Trajectory D leads to the sequence low-voltage – burst-suppression – other patterns, corresponding to Fig. 3D. Trajectory E leads to the sequence low-voltage – burst-suppression – low-voltage, corresponding to Fig. 3E.

1994). For low LTP-values it appears that recovery is still possible. For example, in Fig.3B, some patients with irregular discharges improved to a normal EEG and had a good outcome. However, our clinical EEG data suggest that some evolutionary pathways always lead to a poor outcome. For example, in our dataset none of the patients who developed burst-suppression patterns or periodic discharges survived. This suggests that there may be an LTP threshold value that always leads to a poor outcome, if exceeded. This can be explained by the fact that LTP is a potential cause of secondary neural cell death, for example as a result of excessive postsynaptic calcium influx (Szatkowski and Attwell, 1994).

On the time scales considered in this work, we assumed the LTP of excitatory neurotransmission to be permanent and static. If LTP does not cause excitotoxicity leading to secondary neural death, it is likely that its effect will be reversible. A possible mechanism is synaptic scaling (Turrigiano, 2008). In this form of homeostatic plasticity, excitatory synapses increase or decrease their strength in order to maintain neural firing rates. In order to achieve physiological postsynaptic firing rates, synaptic scaling mechanisms will normalize synaptic strength on a time scale of days. This may explain the fact that, eventually, after days, many EEG patterns observed in postanoxic encephalopathy evolve to continuous patterns, even in patients with a poor outcome (Cloostermans et al., 2012; Jørgensen and Holm, 1998). However, such EEGs are typically characterized by a lower voltage and slower rhythms, presumably resulting from a significant loss of number of synapses of neurons.

4.3. Effect of propofol

The model simulations show that with the application of propofol, for low and intermediate LTP values, irregular and periodic discharges can be suppressed. By enhancement of inhibitory synaptic neurotransmission and inhibition of excitatory neurotransmission, propofol directly antagonizes the effect of long-term potentiation. This finding agees with observations in the clinical EEG data: none of the patients with good outcome, who are supposed to have little or moderate anoxic LTP, showed epileptiform discharges during

propofol treatment On the other hand, propofol application was not sufficient to suppress epileptiform discharges in all number of patients with poor outcome, who presumably have a strong anoxic LTP. The model predicts that the application of propofol only temporarily suppresses periodic discharges, unless the LTP-factor decreases during treatment. It is unlikely that synaptic scaling mechanisms will account for this effect, as propofol treatment normalizes postsynaptic firing rates.

4.4. Generalization of findings

Some of the EEG abnormalities simulated with our model are not unique for postanoxic encephalopathy. For example, GPDs can also be observed in other conditions, most commonly metabolic encephalopathies, CNS infections, and acute stroke. (Foreman et al., 2012). Since the time course of synaptic failure and LTP of excitatory neurotransmission are specific for postanoxic encephalopathy, our model findings cannot be generalized to these conditions. However, all conditions associated with GPDs readily affect synaptic neurotransmission, since it is one of the earliest events in case of energy depletion or metabolic derangements (Hofmeijer and van Putten, 2012). Therefore, it seems likely that GPDs in all these conditions result from (selective) synaptic failure, leading to an imbalance between excitatory and inhibitory neurotransmission.

4.5. Limitations

By construction, a computational model like ours is a simplification of the neural network dynamics underlying the EEG. The main limitation of our model is that spatial aspects are not incorporated. In fact, we only simulated a single EEG channel. We find this reasonable since cerebral perfusion is diffusely affected after cardiac arrest, and EEG patterns in postanoxic coma are typically spatially homogeneous. However, particular phenomena, such as bilateral synchronization of burst suppression patterns, are not explained. Further, the lack of spatial heterogeneities may explain that the model generates a single pathological burst type, only, similar to epileptiform or identical bursts (Hofmeijer et al., 2013). Using the spatio-temporal Liley model one can simulate bursts with physiological burst content, as induced by anesthetic drugs, too (Bojak et al., 2015).

Our model is also limited by some of the assumptions. For example, we did not incorporate the effects of primary or secondary cell death, and neither did we take into account the effects of a disturbed ion balance on the cellular excitability. We assume this reasonable because EEG rhythms mainly represent synaptic currents (Buzsáki et al., 2012). It would, in principle, be possible to account for disturbed ion balance by adjusting the neural activation curve (S-curve) of the model, as was done for example by Zandt et al. (2014). The shape of the neural activation curve used in our model suggests that for high membrane potentials, the population firing rate saturates to its maximum value. However, above a certain membrane potential, a depolarization block can have significant influence on the dynamics (Meijer et al., 2015). We assumed for simplicity that anoxic LTP takes place immediately after cardiac arrest. This is not true, as LTP generally arises in hours. In animal experiments, the maximum increase in excitatory neurotransmission took place 5–10 h after the ischemic event (Miyazaki et al., 1993; Urban et al., 1989). Finally, we assumed that all synapses are affected by hypoxia, and that all excitatory synapses or inhibitory synapses are affected in the same way, including intracortical, cortico-cortical, and thalamocortical synapses. However, experimental evidence shows that the vulnerability depends on the type of cell or synapse (Martin et al., 1994). However, despite these limitations, our model faithfully simulates the main characteristic EEG patterns observed in patients with a postanoxic encephalopathy, and their temporal changes.

4.6. Conclusions

We simulated frequently observed evolving EEG patterns in postanoxic encephalopathy using a neural mean field model. The simulations indicate that aggravation of short-term synaptic depression and potentiation of excitatory neurotransmission play a key role in the pathophysiology of postanoxic encephalopathy and recovery, as well as in the generation of EEG abnormalities. Impairment of synaptic functioning is more pronounced in excitatory than in inhibitory synapses. The model predicts that generalized periodic discharges result from a potentiation of excitatory neurotransmission and are essentially resistant to treatment.

Acknowledgements

We thank the ICU staff and all clinical neurophysiology lab technicians from Medisch Spectrum Twente for the extensive support and constructive collaboration. We thank Marleen C. Tjepkema-Cloostermans for her contribution to the clinical data collection. Barry J. Ruijter was financially supported by the Dutch National Epilepsy Fund (Nationaal Epilepsie Fonds, grant reference NEF 14–18). The funder had no role in study design, data collection and analysis, decision to publish, or preparation of the manuscript.

Conflict of interest statement: None of the authors have potential conflicts of interest to be disclosed.

Appendix A. Model equations and parameters

The spatially homogeneous bursting Liley model consists of eight coupled differential equations:

$$\tau_e \dot{V}_e(t) = V_e^{rest} - V_e(t) + \frac{V_e^{eq} - V_e(t)}{|V_e^{eq} - V_e^{rest}|} I_{ee}(t) + \frac{V_i^{eq} - V_e(t)}{|V_i^{eq} - V_e^{rest}|} I_{ie}(t), \tag{A.1}$$

$$\tau_i \dot{V}_i(t) = V_i^{rest} - V_i(t) + \frac{V_e^{eq} - V_i(t)}{|V_e^{eq} - V_i^{rest}|} I_{ei}(t) + \frac{V_i^{eq} - V_i(t)}{|V_i^{eq} - V_i^{rest}|} I_{ii}(t), \tag{A.2}$$

$$\tilde{I}_{ee}(t) = -(\gamma_e + \tilde{\gamma}_e)\dot{I}_{ee}(t) - \gamma_e \tilde{\gamma}_e I_{ee}(t) + \tilde{\gamma}_e e^{\gamma_e/\gamma_e^0} \Gamma_e(t) \times (N_{ee}^{\beta} S_e(V_e(t)) + p_{ee}(t)), \tag{A.3}$$

$$\tilde{I}_{ei}(t) = -(\gamma_e + \tilde{\gamma}_e)\dot{I}_{ei}(t) - \gamma_e \tilde{\gamma}_e I_{ei}(t) + \tilde{\gamma}_e e^{\gamma_e/\gamma_e^0} \Gamma_e(t) \times (N_{ei}^{\beta} S_e(V_e(t)) + p_{ei}(t)), \tag{A.4}$$

$$\tilde{I}_{ie}(t) = -(\gamma_i + \tilde{\gamma}_i)\dot{I}_{ie}(t) - \gamma_i \tilde{\gamma}_i I_{ie}(t) + \tilde{\gamma}_i e^{\gamma_i/\gamma_i^0} \Gamma_i(t) N_{ie}^{\beta} S_i(V_i(t)), \tag{A.5}$$

$$\tilde{I}_{ii}(t) = -(\gamma_i + \tilde{\gamma}_i)\dot{I}_{ii}(t) - \gamma_i \tilde{\gamma}_i I_{ii}(t) + \tilde{\gamma}_i e^{\gamma_i/\gamma_i^0} \Gamma_i(t) N_{ii}^{\beta} S_i(V_i(t)), \tag{A.6}$$

$$\dot{\Gamma}_e(t) = \frac{\Gamma_e^{rest} - \Gamma_e(t)}{\tau_e^{rec}} - \rho_e^{dep} S_e(V_e(t)) \Gamma_e(t), \tag{A.7}$$

$$\dot{\Gamma}_i(t) = \frac{\Gamma_i^{rest} - \Gamma_i(t)}{\tau_i^{rec}} - \rho_i^{dep} S_i(V_i(t)) \Gamma_i(t). \tag{A.8}$$

Table A.1 gives a physiological interpretation of the parameters and their numerical values. The functions $S_k(V_k)$ and parameters γ_k, $\tilde{\gamma}_k$, Γ_k^{rest}, and p_{ek} (with $k = e, i$) are not listed in the table but will be discussed below. Equations (A.1) and (A.2) determine the dynamics of the mean membrane potentials of the excitatory

Table A.1
Model parameters, their symbols, and default values (see Liley et al., 2002).

Parameter	Symbol	Default values
Mean soma membrane potential	V_e, V_i	n.a.
Mean resting membrane potential	V_e^{rest}, V_i^{rest}	−70 mV, −70 mV
Mean equilibrium potential associated with excitation or inhibition	V_e^{eq}, V_i^{eq}	45 mV, −90 mV
Total number of connections that a cell of type e, i receives from excitatory cells via intracortical fibers	N_{ee}^{β}, N_{ei}^{β}	3000, 3000
Total number of connections that a cell of type e, i receives from inhibitory cells	N_{ie}^{β}, N_{ii}^{β}	500, 500
Excitatory, inhibitory postsynaptic potential peak amplitude	Γ_e^0, Γ_i^0	0.71 mV, 0.71 mV
Excitatory, inhibitory postsynaptic potential rate constant	γ_e^0, γ_i^0	300 s^{-1}, 65 s^{-1}
Passive membrane time constant	τ_e, τ_i	0.094 s, 0.042 s
Excitatory, inhibitory population thresholds	μ_e, μ_i	−50 mV, −50 mV
Excitatory, inhibitory population mean maximal firing rates	S_e^{max}, S_e^{max}	500 s^{-1}, 500 s^{-1}
Mean excitatory input to excitatory, inhibitory cells	p_{ee}, p_{ei}	3460 s^{-1}, 5070 s^{-1}
Standard deviation of excitatory input to excitatory cells	$sd(p_{ee})$	1000 s^{-1}
Inhibitory input to excitatory, inhibitory cells	p_{ie}, p_{ii}	0 s^{-1}, 0 s^{-1}
Standard deviation for firing threshold in excitatory, inhibitory populations	σ_e, σ_i	5 mV, 5 mV
Recovery time constant for activity dependent synaptic depression	τ_e^{rec}, τ_i^{rec}	0.5 s, 0.5 s
Depletion constant for activity dependent synaptic depression	p_e^{dep}, p_i^{dep}	0.003, 0.003

(V_e) and inhibitory (V_i) neural populations, respectively. These potentials depend on the synaptic currents $I_{nm}(t)$ with $n, m = e, i$, described by Eqs. (A.3)–(A.6). Note that in absence of synaptic currents, the mean membrane potentials decay to their resting values V_e^{rest} and V_i^{rest}, respectively. The following *activation functions* relate mean membrane potentials to population firing rates:

$$S_e(V_e) = \frac{Q_e^{\max}}{1 + e^{-\sqrt{2}(V_e-\mu_e)/\sigma_e}}, \tag{A.9}$$

$$S_i(V_i) = \frac{Q_i^{\max}}{1 + e^{-\sqrt{2}(V_i-\mu_i)/\sigma_i}}. \tag{A.10}$$

The system of equations is driven by white noise input, incorporated via p_{ee}. This parameter is defined as $p_{ee} = \bar{p}_{ee} + p_{ee}^*$, where $\bar{p}_{ee}$ is the mean excitatory external input and p_{ee}^* white noise with standard deviation $sd(p_{ee})$. The external excitatory input to inhibitory synapses (p_{ei}) is constant: $p_{ei} = \bar{p}_{ei}$.

For our simulations, we chose a set of baseline parameter values that result in a physiological alpha rhythm. These values were used before in (Liley et al., 2002) and (Tjepkema-Cloostermans et al., 2014) and are shown in Table A.1. We used the mean membrane potential of the excitatory population $V_e(t)$ as 'EEG signal', as was done in for example (Bojak et al., 2015).

A.1. Synaptic time constants (γ_k and $\tilde{\gamma}_k$)

Without anesthetics, the rise and decay times of the postsynaptic potentials are dictated by the baseline synaptic time constant γ_k^0. The bursting Liley model assumes that anesthetics only affect the decay rate of the inhibitory postsynaptic potential. To alter the decay rate without changing the rise rate, the time constants γ_k and $\tilde{\gamma}_k$ are introduced, as was done for the first time in (Bojak and Liley, 2005):

$$\gamma_k \equiv \frac{\gamma_k^0 \varepsilon_k(c)}{e^{\varepsilon_k(c)} - 1}, \quad \tilde{\gamma}_k \equiv e^{\varepsilon_k(c)}\gamma_k, \tag{A.11}$$

where $\varepsilon_k(c)$ is a monotonically increasing function of the anesthetics concentration c. With this parameterization, anesthetics increase the PSP decay time, without affecting its rise time. In the limit $c \to 0$, indicating no treatment with anesthetics, $\varepsilon_k(c) \to 0$ and $\gamma_k = \tilde{\gamma}_k = \gamma_k^0$.

In our model, we aimed to model the effects of propofol. Although $\varepsilon_k(c)$ is quantitatively based on the effects of isoflurane (Bojak and Liley, 2005), we assumed propofol to have the same qualitative effects, since the GABAA receptor is the most important target site of both drugs (Garcia et al., 2010).

A.2. Resting value of the maximum postsynaptic potential (Γ_k^{rest})

Assuming that the system of equations starts at equilibrium at $t = 0$ with $V_k(t = 0) = V_k^0$ and $\Gamma_k(t = 0) = \Gamma_k^0$, it follows from Eqs. (A.7) and (A.8) that the resting value of the maximum postsynaptic potential is (Bojak et al., 2015):

$$\Gamma_k^{rest} = \Gamma_k^0(1 + \tau_k^{rec}\rho_k^{dep}S_k(V_k^0))H_k(c), \tag{A.12}$$

with $0 \leqslant H_k(c) \leqslant 1$ a Hill function depending on the concentration c of anesthetic agent:

$$H_e(c) = \frac{0.707^{2.22}}{0.707^{2.22} + c^{2.22}}, \tag{A.13}$$

$$H_i(c) = \frac{0.79^{2.6} + 0.56c^{2.6}}{0.79^{2.6} + c^{2.6}}. \tag{A.14}$$

This function is quantitatively based on the effects of isoflurane (Bojak and Liley, 2005). Note that EPSP amplitudes are more reduced by anesthetics than IPSP amplitudes.

For our simulations, we made a few adaptations to the equations above. First, we assumed the Hill Eqs. (A.13) and (A.14) of isoflurane to hold qualitatively for propofol. Then, we multiplied postsynaptic potentials with $G_k(LTP) \geqslant 1$, a function of the long term potentiation factor LTP:

$$G_e(LTP) = 1 + LTP, \tag{A.15}$$

$$G_i(LTP) = 1. \tag{A.16}$$

So, only excitatory synapses are affected by anoxic long term potentiation. Finally, for computational efficiency, we made the approximation $\Gamma_k^0(1 + \tau_k^{rec}\rho_k^{dep}S_k(V_k^0)) \approx \Gamma_k^0$. This approximation did not qualitatively influence the simulation results. The final expression for the resting value of the maximum postsynaptic potential in our model was therefore

$$\Gamma_k^{rest} = \Gamma_k^0 H_k(c) G_k(LTP). \tag{A.17}$$

Appendix B. Mathematical description of transitions between simulated EEG patterns

The transitions between simulated EEG patterns can also be described mathematically. Let us consider the numbered areas in Fig.5A. If we start in region 2a, i.e. the hyperpolarized state, we find a stable steady state. Adding (sensory) noise yields small fluctuations. Moving towards region 3 the fluctuations become larger in amplitude. Next when moving into region 1, the steady state exhibits a supercritical Hopf bifurcation such that stable oscillations occur in the absence of inputs. With noise the fluctuations increase

in amplitude. This illustrates that the demarcations of these regions are slightly arbitrary. The transition from region 1 to 5 reveals a drastic change in excitability. In region 5, the fluctuations resemble those of region 1, but here they may evoke an occasional spike by the noise. Moving from region 5 to 6, the small oscillation is no longer stable through a saddle-node bifurcation. From region 6 to region 2b we find again a supercritical Hopf bifurcation which results in depolarization block. In between, we find burst-suppression patterns in regions 4a/b. The specific bursting pattern is of subHopf/fold cycle-type. See also (Izhikevich, 2000).

Appendix C. Supplementary material

Supplementary data associated with this article can be found, in the online version, at http://dx.doi.org/10.1016/j.clinph.2017.06.245.

References

Bodsch W, Barbier A, Oehmichen M, Grosse Ophoff B, Rossmann K-A. Recovery of monkey brain after prolonged ischemia. II. Protein synthesis and morphological alteraltions. J Cereb Blood Flow Metab 1986;6:15–21. http://dx.doi.org/10.1038/jcbfm.1986.3.

Bojak I, Liley DTJ. Modeling the effects of anesthesia on the electroencephalogram. Phys Rev E 2005;71:1–22. http://dx.doi.org/10.1103/PhysRevE.71.041902.

Bojak I, Stoyanov ZV, Liley DT. Emergence of spatially heterogeneous burst suppression in a neural field model of electro cortical activity. Front Syst Neurosci 2015;9:1–20. http://dx.doi.org/10.3389/fnsys.2015.00018.

Bolay H, Gürsoy-Özdemir Y, Sara Y, Onur R, Can A, Dalkara T. Persistent defect in transmitter release and synapsin phosphorylation in cerebral cortex after transient moderate ischemic injury. Stroke 2002;33:1369–75. http://dx.doi.org/10.1161/01.STR.0000013708.54623.DE.

Buzsáki G, Anastassiou CA, Koch C. The origin of extracellular fields and currents – EEG, ECoG, LFP and spikes. Nat Rev Neurosci 2012;13:407–20. http://dx.doi.org/10.1038/nrn3241.

Calabresi P, Centonze D, Pisani A, Cupini LM, Bernardi G. Synaptic plasticity in the ischaemic brain. Lancet Neurol 2003;2:622–9. http://dx.doi.org/10.1016/S1474-4422(03)00532-5.

Cloostermans MC, van Meulen FB, Eertman CJ, Hom HW, van Putten MJAM. Continuous electroencephalography monitoring for early prediction of neurological outcome in postanoxic patients after cardiac arrest: A prospective cohort study. Crit Care Med 2012;40:2867–75. http://dx.doi.org/10.1097/CCM.0b013e31825b94f0.

Coombes S. Large-scale neural dynamics: simple and complex. Neuroimage 2010;52:731–9. http://dx.doi.org/10.1016/j.neuroimage.2010.01.045.

Deco G, Jirsa VK, Robinson PA, Breakspear M, Friston K. The dynamic brain: from spiking neurons to neural masses and cortical fields. PLoS Comput Biol 2008;4. http://dx.doi.org/10.1371/journal.pcbi.1000092.

Foreman B, Claassen J, Khaled K. Generalized periodic discharges in the critically ill A case-control study of 200 patients. Neurology 2012:1951–60. http://dx.doi.org/10.1212/WNL.0b013e3182735cd7.

Garcia PS, Kolesky SE, Jenkins A. General anesthetic actions on GABA(A) receptors. Curr Neuropharmacol 2010;8:2–9. http://dx.doi.org/10.2174/157015910790909502.

Goodfellow M, Schindler K, Baier G. Intermittent spike – wave dynamics in a heterogeneous, spatially extended neural mass model. Neuroimage 2011;55:920–32. http://dx.doi.org/10.1016/j.neuroimage.2010.12.074.

Hammond C, Crépel V, Gozlan H, Ben-Ari Y. Anoxic LTP sheds light on the multiple facets of NMDA receptors. Trends Neurosci 1994;17:497–503. http://dx.doi.org/10.1016/0166-2236(94)90140-6.

Hofmeijer J, Beernink TMJ, Bosch FH, Beishuizen A, Tjepkema-Cloostermans MC, Van Putten MJAM. Early EEG contributes to multimodal outcome prediction of postanoxic coma. Neurology 2015;85:137–43. http://dx.doi.org/10.1212/WNL.0000000000001742.

Hofmeijer J, Mulder ATB, Farinha AC, Van Putten MJAM, Le Feber J. Mild hypoxia affects synaptic connectivity in cultured neuronal networks. Brain Res 2014;1557:180–9. http://dx.doi.org/10.1016/j.brainres.2014.02.027.

Hofmeijer J, van Putten MJAM. Ischemic cerebral damage: an appraisal of synaptic failure. Stroke 2012;43:607–15. http://dx.doi.org/10.1161/STROKEAHA.111.632943.

Hofmeijer J, Tjepkema-Cloostermans MC, van Putten MJAM. Burst-suppression with identical bursts: a distinct EEG pattern with poor outcome in postanoxic coma. Clin Neurophysiol 2013;125:947–54. http://dx.doi.org/10.1016/j.clinph.2013.10.017.

Ikeda M, Nakazawa T, Abe K, Kaneko T, Yamatsu K. Extracellular accumulation of glutamate in the hippocampus induced by ischemia is not calcium dependent – in vitro and in vivo evidence. Neurosci Lett 1989;96:202–6. http://dx.doi.org/10.1016/0304-3940(89)90058-X.

Izhikevich EM. Neural excitability, spiking and bursting. Int J Bifurc Chaos 2000;10:1171–266.

Jørgensen E, Holm S. The natural course of neurological recovery following cardiopulmonary resuscitation. Resuscitation 1998;36:111–22. http://dx.doi.org/10.1016/S0300-9572(97)00094-4.

Khazipov R, Congar P, Ben-Ari Y. Hippocampal CA1 lacunosum-moleculare interneurons: comparison of effects of anoxia on excitatory and inhibitory postsynaptic currents. J Neurophysiol 1995;74:2138–49.

Liley DTJ, Cadusch PJ, Dafilis MP. A spatially continuous mean field theory of electrocortical activity. Network 2002;13:67–113. http://dx.doi.org/10.1088/0954-898X/14/2/601.

Liley DTJ, Walsh M. The mesoscopic modeling of burst suppression during anesthesia. Front Comput Neurosci 2013;7:46. http://dx.doi.org/10.3389/fncom.2013.00046.

Ljunggren B, Ratcheson RA, Siesjö BK. Cerebral metabolic state following complete compression ischemia. Brain Res 1974;73:291–307. http://dx.doi.org/10.1016/0006-8993(74)91050-6.

Martin RL, Lloyd HGE, Cowan AI. The early events of oxygen and glucose deprivation: setting the scene for neuronal death? Trends Neurosci 1994;17:251–7. http://dx.doi.org/10.1016/0166-2236(94)90008-6.

Meijer HGE, Eissa TL, Kiewiet B, Neuman JF, Schevon CA, Emerson RG, et al. Modeling focal epileptic activity in the Wilson-cowan model with depolarization block. J Math Neurosci 2015;5:7. http://dx.doi.org/10.1186/s13408-015-0019-4.

Miyazaki S, Katayama Y, Furuichi M, Kinoshita K, Kawamata T, Tsubokawa T. Post-ischemic potentiation of Schaffer collateral/CA1 pyramidal cell responses of the rat hippocampus in vivo: involvement of N-methyl-D-aspartate receptors. Brain Res 1993;611:155–9. http://dx.doi.org/10.1016/0006-8993(93)91788-T.

Naruse S, Horikawa Y, Tanaka C, Hirakawa K, Nishikawa H, Watari H. In vivo measurement of energy metabolism and the concomitant monitoring of electroencephalogram in experimental cerebral ischemia. Brain Res 1984;296:370–2.

Nielsen N, Wetterslev J, Cronberg T, Erlinge D, Gasche Y, Hassager C, et al. Targeted temperature management at 33 C versus 36 C after cardiac arrest. N Engl J Med 2013;369:2197–206. http://dx.doi.org/10.1056/NEJMoa1310519.

Oh SH, Park KN, Shon YM, Kim YM, Kim HJ, Youn CS, et al. Continuous amplitude-integrated electroencephalographic monitoring is a useful prognostic tool for hypothermia-treated cardiac arrest patients. Circulation 2015;132:1094–103. http://dx.doi.org/10.1161/CIRCULATIONAHA.115.015754.

Robinson PA, Rennie CJ, Rowe DL. Dynamics of large-scale brain activity in normal arousal states and epileptic seizures. Phys Rev E 2002;65:1–9. http://dx.doi.org/10.1103/PhysRevE.65.041924.

Rossi DJ, Oshima T, Attwell D. Glutamate release in severe brain ischaemia is mainly by reversed uptake. Nature 2000;403:316–21. http://dx.doi.org/10.1038/35002090.

Ruijter BJ, van Putten MJAM, Hofmeijer J. Generalized epileptiform discharges in postanoxic encephalopathy: quantitative characterization in relation to outcome. Epilepsia 2015;56:1845–54. http://dx.doi.org/10.1111/epi.13202.

Siesjö BK, Elmer E, Janelidze S, Keep M, Kristian T, Ouyang YB, et al. Role and mechanisms of secondary mitochondrial failure. Acta Neurochir Suppl 1999;73:7–13.

Somjen GG. Mechanisms of early, reversible hypoxic synaptic failure. Ions Brain Norm. Funct. seizures stroke. Oxford University Press; 2004. p. 327–37.

Szatkowski M, Attwell D. Triggering and execution of neuronal death in brain ischaemia: two phases of glutamate release by different mechanisms. Trends Neurosci 1994;17:359–65. http://dx.doi.org/10.1016/0166-2236(94)90040-X.

Tabak J, Senn W, O'Donovan MJ, Rinzel J. Modeling of spontaneous activity in developing spinal cord using activity-dependent depression in an excitatory network. J Neurosci 2000;20:3041–56.

Tjepkema-Cloostermans MC, Hindriks R, Hofmeijer J, van Putten MJAM. Generalized periodic discharges after acute cerebral ischemia: Reflection of selective synaptic failure? Clin Neurophysiol 2014;125:255–62. http://dx.doi.org/10.1016/j.clinph.2013.08.005.

Tjepkema-Cloostermans MC, Hofmeijer J, Trof RJ, Blans MJ, Beishuizen A, van Putten MJAM. Electroencephalogram predicts outcome in patients with postanoxic coma during mild therapeutic hypothermia. Crit Care Med 2015;43:159–67. http://dx.doi.org/10.1097/CCM.0000000000000626.

Tjepkema-Cloostermans MC, van Meulen FB, Meinsma G, van Putten MJ. A Cerebral Recovery Index (CRI) for early prognosis in patients after cardiac arrest. Crit Care 2013;17:R252. http://dx.doi.org/10.1186/cc13078.

Tsodyks M, Markram H. The neural code between neocortical pyramidal neurons depends. Proc Natl Acad Sci 1997;94:565–8.

Turrigiano GG. The self-tuning neuron: synaptic scaling of excitatory synapses. Cell 2008;135:422–35. http://dx.doi.org/10.1016/j.cell.2008.10.008.

Urban L, Neill KH, Crain BJ, Nadler JV, Somjen GG. Postischemic synaptic physiology in area CA1 of the gerbil hippocampus studied in vitro. J Neurosci 1989;9:3966–75.

Wendling F, Bartolomei F, Bellanger JJ, Chauvel P. Epileptic fast activity can be explained by a model of impaired GABAergic dendritic inhibition. Eur J Neurosci 2002;15:1499–508. http://dx.doi.org/10.1046/j.1460-9568.2002.01985.x.

Wijdicks E, Young G. Myoclonus status in comatose patients after cardiac arrest. Lancet 1994;343:1642–3.

Young GB, Gilbert JJ, Zochodne DW. The significance of myoclonic status epilepticus in postanoxic coma. Neurology 1990;40:1843–8. http://dx.doi.org/10.1212/WNL.40.12.1843.

Zandt B-J, Visser S, Putten MJ, Ten Haken B. A neural mass model based on single cell dynamics to model pathophysiology. J Comput Neurosci 2014;37:549–68. http://dx.doi.org/10.1007/s10827-014-0517-5.